

# Sector Workload Model for Benefits Analysis and Convective Weather Capacity Prediction

Jerry D. Welch, John Y. N. Cho, Ngaire K. Underhill, and Richard A. DeLaura

MIT Lincoln Laboratory

Lexington, Massachusetts, U.S.A.

welch@LL.MIT.EDU, jyinc@LL.MIT.EDU, ngaire.underhill@LL.MIT.EDU, richd@LL.MIT.EDU

**Abstract**— En route sector capacity is determined mainly by controller workload. The operational capacity model used by the Federal Aviation Administration (FAA) provides traffic alert thresholds based entirely on hand-off workload. Its estimates are accurate for most sectors. However, it tends to over-estimate capacity in both small and large sectors because it does not account for conflicts and recurring tasks. Because of those omissions it cannot be used for accurate benefits analysis of workload-reduction initiatives, nor can it be extended to estimate capacity when hazardous weather increases the intensity of all workload types.

We have previously reported on an improved model that accounts for all workload types and can be extended to handle hazardous weather. In this paper we present the results of a recent regression of that model using an extensive database of peak traffic counts for all United States en route sectors. The resulting fit quality confirms the workload basis of en route capacity. Because the model has excess degrees of freedom, the regression process returns multiple parameter combinations with nearly identical sector capacities. We analyze the impact of this ambiguity when using the model to quantify the benefits of workload reduction proposals. We also describe recent modifications to the weather-impacted version of the model to provide a more stable normalized capacity measure. We conclude with an illustration of its potential application to operational sector capacity forecasts in hazardous weather.

*Keywords-workload; capacity; enroute; sector; weather*

## I. INTRODUCTION

The capacity of en route sectors is determined more by controller workload than by airspace limitations [1]. We have found that this is also often true in sectors that are partially blocked by hazardous weather. A model based on the premise that the weather increases controller workload can explain observed reductions in traffic during historical storm events [2].

A workload-based model is also useful for the analysis of the capacity benefits of any proposed air traffic management improvement aimed at reducing controller workload [3, 4]. Examples include digital data communication, improved surveillance accuracy and update rates, decision support automation for controllers, conflict prevention/resolution

systems, self-separation aids for pilots, and systems for improved weather sensing, predicting, and avoidance.

Accurate capacity models are also needed to manage operational flow as traffic demand grows or as hazardous weather introduces additional controller tasks [5, 6]. The current FAA capacity model provides operational traffic alerts based solely on hand-off workload without considering conflict-resolution, recurring, and background tasks [7]. This approach is effective and simple because inter-sector coordination workload dominates most sectors and grows linearly with traffic count. It is inversely related to the mean transit time of the traffic through a sector, and we thus refer to it as “transit” workload.

Sector size also affects capacity. Small sectors are expressly designed to handle dense airspace by allowing more persons to cooperate in its control. However, small sectors have less individual peak traffic handling capacity than large sectors, partly because of reduced transit times and partly because of higher conflict rates. Conflict-prevention and resolution workload grows linearly with traffic density and ultimately dominates small sectors operating near capacity.

Large sectors have larger mean transit times, which tend to offset the effect of traffic growth on transit workload. However, recurring tasks such as traffic monitoring increase linearly with traffic, and are independent of transit time. Thus, recurring tasks dominate large sectors that operate near capacity. Consequently, a model that considers only transit workload has a tendency to over-estimate capacity in both small and large sectors.

Another limitation of a model that does not consider conflict or recurring tasks is that it cannot be extended to estimate sector capacity when weather forces controllers to reduce aircraft separations and to vector aircraft around storm cells.

We have developed a model that accounts for all task types [8]. It defines four aggregated workload components. One component includes tasks that increase as the square of the traffic count,  $N$ . Two others include tasks that increase linearly with  $N$ , and one is independent of  $N$ . The capacity of the sector is defined as the value of  $N$  that makes the sum of the four

workload components equal an empirically determined safe workload intensity limit.

We begin this paper by reviewing the FAA’s current operational sector overload alerting tool, which uses a subset of the full model. We follow with a short review of how workload models determine traffic flow capacity and support strategic air traffic management based on directional flow. We then review the full workload model and show results from a recent data regression using a large and comprehensive database of peak traffic counts for all en route sectors in the United States. The quality of the fit confirms the workload basis of en route capacity and the ability of four workload components to quantify that capacity

The full model has extra degrees of freedom that result in multiple combinations of regression parameters that give nearly identical sector capacities but distinctly different workload ratios. We address the impact of these parameter ambiguities on benefits analyses that must distinguish between different workload types.

We conclude by describing improvements to our extension of the model that allow estimation of the reduction of a sector’s operational capacity resulting from a partial blockage of its airspace by hazardous weather. Such estimates could provide operational alerts based on forecasts of en route sector demand relative to the current capacity estimates for those sectors. The added alerts would indicate sector-capacity percentage reduction relative to the full-workload sector capacity estimates in fair weather.

We outline the procedure for computing the fractional en route sector volume weather blockage, and for using that metric to estimate the residual capacity of the sector. We conclude with an illustration using archived traffic and weather data to simulate an operational weather alerting procedure.

## II. WORKLOAD CAPACITY MODELS

### A. Monitor Alert Parameter (MAP) Model

It is informative to illustrate the underlying theory of sector capacity in the simpler context of the FAA’s current operational National Airspace System (NAS) Monitor Alert tool. We start with the definition of workload intensity, which is the fraction of the sector controller team’s time that is occupied with a given task type. The workload intensity associated with a task type is the product of the mean time required to service that type of task and the mean task rate [1].

Analysis of the FAA’s MAP capacity rule [7] shows that it bases sector capacity alerting thresholds on an implicit workload model that considers only transit workload intensity,

$$G_t = \tau_t \frac{N_{MAP}}{T}. \quad (1)$$

The MAP capacity model is consistent with an observation that the mean hand-off service time  $\tau_t$  is 36 seconds and that each sector reaches capacity when its workload intensity  $G_t$  equals 1. To find the peak allowable aircraft count for any sector, we set  $G_t = 1$  and solve for the MAP capacity  $N_{MAP}$ . When  $G_t$  equals 1,  $N_{MAP} = T/36$ . Thus,  $N_{MAP}$  is proportional to  $T$ , and when  $T = 360$  seconds, the MAP capacity is 10 aircraft.

Operational experience indicates that the safe capacity of an en route sector does not continue to increase linearly as  $T$  increases beyond about 600 seconds. For this reason, the MAP rule includes an upper capacity limit of 18 aircraft. Operational experience also indicates that factors other than transit time can influence each sector’s capacity. Consequently, the MAP rule allows operational settings to deviate from the nominal rule by plus or minus three aircraft.

Although the current MAP operational settings are static, the MAP model could provide dynamic fair-weather capacity estimates if it were provided with current or predicted sector transit times, which change with prevailing winds and current route utilization.

Fig. 1 shows the static MAP operational settings for 680 continental en route sectors in the NAS. The settings lie below the  $N_{MAP} + 3$  upper limit for most sectors except for sectors with mean transit times shorter than 600 seconds.

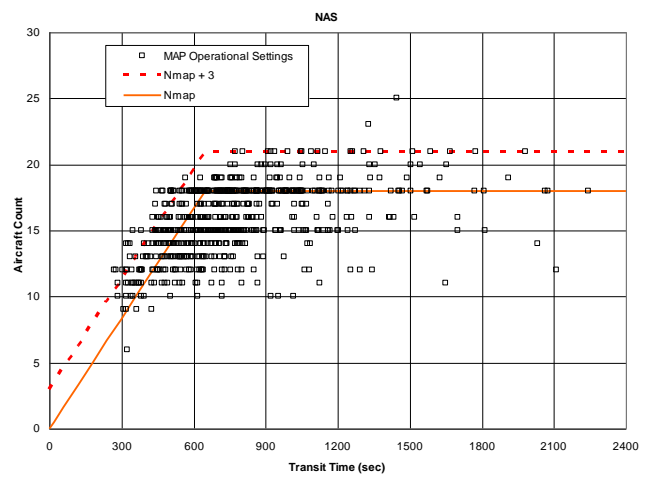


Figure 1. MAP rule and operational MAP settings.

Fig. 2 shows observed peak instantaneous traffic counts for all en route NAS sectors on their peak traffic days in July and August 2007. The counts are plotted versus the mean sector transit time at the time of the count. The frontier slope of the data exceeds the slope implied by the MAP model by about 10%.

Peak counts for a few sectors with transit times greater than 600 seconds exceed the MAP model limit. However, peak counts for most sectors fall well below the MAP model limit. This is appropriate since the MAP model is intended to define a maximum capacity limit for safe operation. Analysis of peak count data indicates that only about 10% of en route sectors ever operate at the MAP model limit. Most of those sectors are located near dense terminal airspace and are manned by skilled controllers. Thus, the workload-based MAP capacity model defines peak instantaneous sector counts that represent current best practice in the U.S. NAS. In fact, capacity estimates from the full workload model suggests that operational MAP settings consistently over-estimate the safe capacity of high traffic density sectors smaller than about 8,000 cubic nautical miles.

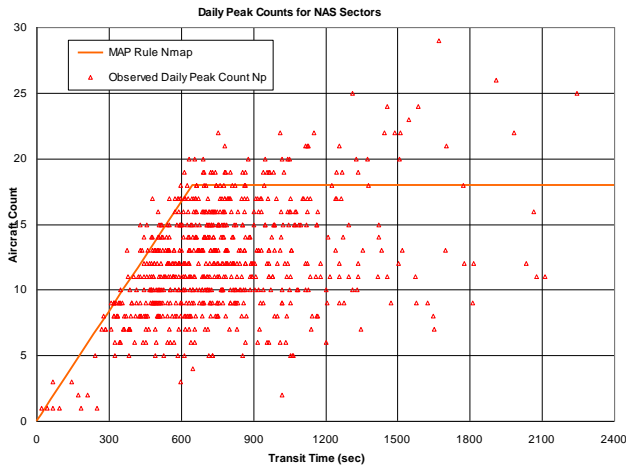


Figure 2. MAP rule and NAS peak sector traffic.

### B. Flow Capacity

Although air traffic managers use sector count  $N$  to monitor potential overloads, they use flow rate  $F$  to control traffic [9, 10]. Sector flow rate is numerically equal to the sector handoff rate, that is, the current sector traffic count  $N$  divided by the mean transit time  $T$  [1].

The black trace in Fig. 3 is a plot of MAP throughput  $F_{MAP}$  versus  $T$ . The linear region of the graph, up to transit times of about 11 minutes, corresponds to a throughput of one flight per 36 seconds, or 100 flights per hour. The observed throughput, which is based on the same peak count and mean transit time data used in Fig. 2, is influenced by the MAP limit, even though flow rates of sectors often exceed the MAP throughput value.

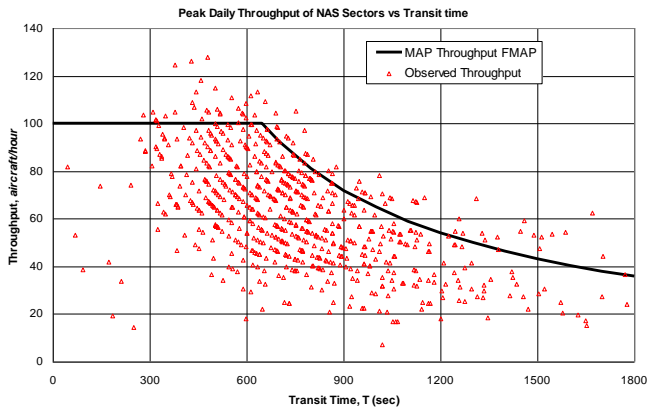


Figure 3. MAP and observed peak throughput for NAS sectors.

The observed decline in throughput for large transit times is evidently caused by the 18-aircraft limit. That decline rate is slightly faster than predicted for those same sectors by the full workload model, as shown in Fig. 4. The full capacity model predicts a small but significant change in flow capacity with sector volume. Very small sectors and very large sectors both tend to constrain flow capacity. Flow capacity peaks at about 120/hr at a sector volume of 5,000 cubic nautical miles and gradually drops to about 70/hr at a volume of 80,000 cubic

nautical miles. It drops to about 50/hr as the sector volume falls to 2,000 cubic nautical miles.

Throughput falls in small sectors because of conflict workload. Small sectors provide an organized way for additional controllers to share the control of airspace that experiences high traffic densities. The sectors with the greatest flow capacities range from 5,000 to 30,000 cubic nautical miles. The most common NAS en route sector volume is 10,000 cubic nautical miles. Although throughput falls in larger sectors because of recurring workload, the decline is of little concern because large sectors are expressly designed for staffing efficiency when controlling airspace with low demand.

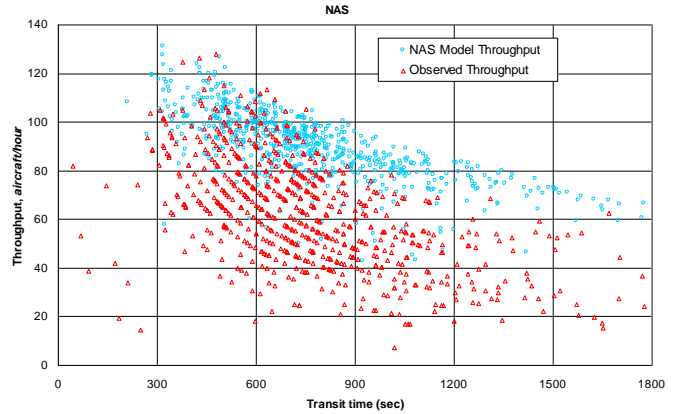


Figure 4. Modeled and observed peak throughput for NAS sectors.

Air traffic managers must also determine the flow capacity of areas encompassing multiple sectors. Since flow is continuous along each route, route flow capacity is determined by the sector along the route with the lowest flow capacity. The flow capacity of any area is simply the sum of the “bottleneck” flow rates for its routes. Smaller sectors compensate for their lower flow capacities by allowing a greater number of routes through a given area.

### C. Flow Directionality

Although sector capacity varies with flow direction, workload-based capacity models do not *explicitly* address directionality. However, workload models incorporate implicit directionality via the mean sector transit time  $T$ . Transit time is the dominant workload factor. Transit time varies with the flow direction relative to wind and relative to sector boundaries. Although the current MAP model employs static, rather than dynamic, transit time estimates, transit time could be estimated from filed flight plans as part of the operational NAS Monitor demand modeling process.

Directionality becomes particularly important in convective weather with “organized” line-storm blockages [11]. Sector workload models do not provide a means of explicitly determining directional capacity in the presence of organized hazardous weather.

### D. Full Workload Model

All sector workload events can be aggregated into workload types that are either independent of traffic (i.e., background workload) or that increase linearly or as the square of the sector

aircraft count  $N$ . As noted above, each workload intensity component is the product of the mean time required to service that type of task and the mean task rate [12].

The conflict rate is proportional to  $N$  squared and inversely proportional to sector airspace volume [1]. The transit rate, as noted previously, is proportional to  $N$  and inversely proportional to the mean transit time of flights through the sector. The recurring workload intensity associated with activities like monitoring and vectoring aircraft is also proportional to  $N$ , but is independent of transit time.

The total workload intensity  $G$  is the fraction of controller time needed to handle constant background workload plus the three task types that increase with  $N$ . When  $N$  grows and  $G$  reaches a limit  $G_c$  such that the controller team cannot safely handle more aircraft, capacity is reached.

The equation for total fair-weather workload intensity is:

$$G = G_b + \frac{\tau_r}{P}N + \frac{\tau_t}{T}N + \frac{BN}{Q}(N + 1), \quad (2)$$

where  $G_b$  is the constant background workload,  $\tau_r$  is the fair-weather recurring task controller service time per flight,  $N$  is the number of flights in the sector,  $P$  is the mean task recurrence period,  $\tau_t$  is the fair-weather inter-sector hand-off service time per flight,  $T$  is the mean sector transit time,  $Q$  is the total sector airspace volume,

$$B = 2M_hM_vV_{12}\tau_c, \quad (3)$$

where  $M_h$  and  $M_v$  are the horizontal and vertical miss distances that constitute a separation violation,  $V_{12}$  is the mean of the pair-wise closing speeds of the aircraft in the sector that could pass closer than the defined miss distances [1], and  $\tau_c$  is the conflict resolution task service time per flight. Physically,  $V_{12}\tau_c$  is the mean separation lost while resolving each conflict, where we refer to the product  $V_{12}\tau_c$  as  $dc$ .

If all aircraft in a sector were flying at constant altitude,  $M_v$  would be constant. Since altitude changes increase the vertical positional uncertainty of the aircraft, we increase  $M_v$  proportionally to the fraction of flights that are ascending or descending in the sector. Specifically, we set

$$M_v = 1 + F_{ca}(M_{vmax} - 1), \quad (4)$$

where  $F_{ca}$  is the fraction of flights in the sector that change altitude by more than 2,000 ft and  $M_{vmax}$  is the maximum vertical miss distance.

Setting  $G$  to  $G_c$ , the human workload limit, and solving equation (1) we get the sector capacity

$$N_m = -\frac{b}{2a} + \frac{1}{2a}\sqrt{b^2 - 4ac}, \quad (5)$$

where

$$a = \frac{B}{Q}, \quad (6)$$

$$b = \frac{\tau_r}{P} + \frac{\tau_t}{T} + a, \quad (7)$$

and

$$c = G_b - G_c, \quad (8)$$

where, as per [12], we set

$$G_c = 0.8. \quad (9)$$

In summary, the independent sector variables that determine the model capacity  $N_m$  are transit time  $T$ , airspace volume  $Q$ , and altitude change fraction  $F_{ca}$ .

### E. NAS Regression

Given the above independent sector variables, we regress against observed peak sector count data to provide numerical values for four key workload model parameters. These are the mean transit service time  $\tau_r$ , the mean loss of separation while servicing conflicts  $dc = \tau_cV_{12}$ , the mean recurring service time  $\tau_r$ , and the maximum vertical miss distance  $M_{vmax}$ . We arbitrarily set the background workload intensity  $G_b$  equal to 0.1 and the mean task recurrence period  $P$  equal to 600 seconds.

We previously reported two trial regressions. The first used data from Northeastern United States airspace, but with sector volumes that did not accurately represent operational sectors [1]. The second used a small data set covering the entire NAS that was restricted to the months of July and Aug 2007 and thus missed high-demand days for centers with peak traffic in winter [13, 14]. (This is the source of the peak sector counts shown in Figs. 2-4.)

The most recent NAS regression is based on data from the ten highest traffic days for each en route center in 2007. This totals 9,170 en route NAS sector-days. It uses archived FAA Sector Design and Analysis Tool (SDAT) data [15] for each of the 20 NAS en route centers. The SDAT database also includes traffic counts from Terminal Radar Approach Control (TRACON) airspace, where extra controller staffing, reduced speeds, and special airspace designs increase capacity beyond en route levels.

The SDAT database provides sector entry and exit times from which we compute the peak instantaneous daily traffic count  $N_p$  and the mean transit time  $T$  of the counted aircraft. The database also provides the current sector area  $A_s$ , and its actual traffic altitudes. We use these to compute the sector airspace volume,  $Q$ . Finally, it provides the daily sector altitude change fraction  $F_{ca}$ . Neither of the earlier trial data sets allowed accurate determination of  $F_{ca}$ .

Fig. 5 shows the SDAT NAS peak instantaneous daily traffic counts  $N_p$  for all sector-days plotted versus the mean transit times  $T$  of the counted aircraft on those days. A distinct upper data frontier is apparent, and it has approximately the same initial slope as that of the limited data set shown in Fig. 2. Other than the number of sector-days, the main difference is the presence of high TRACON traffic counts with sector transit times ranging roughly from 400 to 900 seconds.

Considerable variance or ‘‘spread’’ occurs in the peak counts at all transit times. Many of the peak counts fall below the upper data frontier because of low demand. Low peak counts can also result from small sector volumes or sectors with high altitude-change fractions or sectors with other complexity factors that increase workload and reduce capacity. Numerous such factors have been identified [16 -21]. A key premise of the current model is that all of these workload

factors can be aggregated into four basic workload types, and the degree to which the model fits the data is a test of that premise.

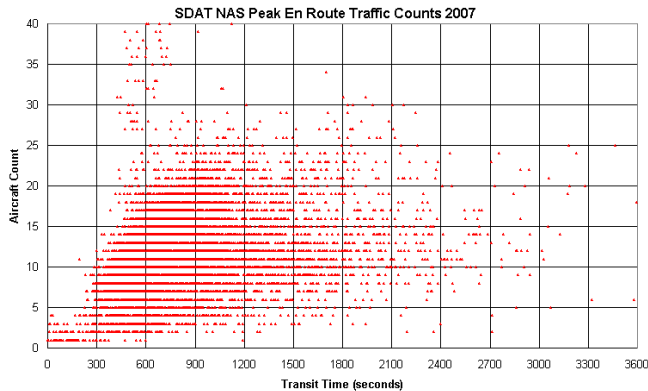


Figure 5. SDAT NAS peak daily traffic count  $N_p$  versus transit time  $T$ .

The regression objective function [14] is designed to focus on the upper data frontier and ignore low-demand sectors ( $N_p < N_m - 4$ ) and high-count TRACON sectors ( $N_p > N_m + 4$ ). It rewards sectors whose counts are equal to or slightly below model capacity, and it penalizes sectors whose counts are slightly above model capacity. We start the regression process by adjusting the reward/penalty ratio to obtain the desired percentile fit.

Our most recent regression resulted in 94.95% of the NAS sectors with peak daily counts less than or equal to their model capacities. It returned a global peak solution associated with the following parameters:  $\tau_i = 14$  seconds,  $dc = 1.6$  nautical miles,  $\tau_r = 9$  seconds, and  $M_{vmax} = 1.6$  nautical miles. These parameters give a mean model capacity for all NAS en route sectors of 17.8 aircraft.

The resulting sector capacities  $N_m$  are plotted in Figs. 6, 7, and 8 versus the three independent sector variables  $T$ ,  $Q$ , and  $F_{ca}$ . All of the capacity plots exhibit upper frontiers that match the corresponding peak count frontiers. There is considerable spread in the model capacity values, but, unlike the spread in the peak counts, it cannot be attributed to lack of demand. It is caused by variations in the other independent variables used to compute the model capacity.

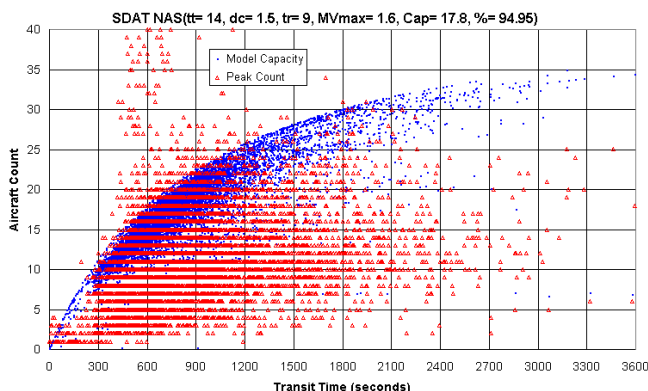


Figure 6. Model capacity  $N_m$  and peak count  $N_p$  versus transit time  $T$ .

The plot of model capacity versus transit time (Fig. 6) has a spread that exhibits a distinct upper bound for all values of  $T$ . This variance is caused by differences in sector size. The highest model capacities are associated with large sectors, but when sector size increases to the point that conflict workload becomes smaller than transit workload, the capacity saturates and is determined solely by  $T$ .

A saturated upper capacity bound also occurs in Fig. 7, but only in very small sectors where conflict workload dominates. Differences in transit workload are the dominant cause of variance in all larger sectors, and the spread grows with  $T$ , which is not bounded.

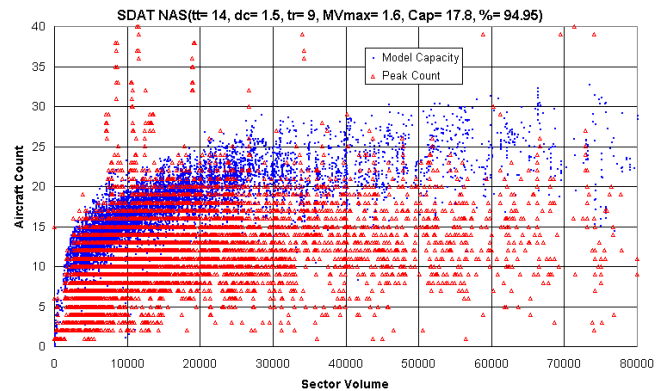


Figure 7.  $N_m$  and  $N_p$  versus sector volume  $Q$ .

Transit workload differences also dominate the plot of model capacity versus altitude change fraction in Fig. 8. The model variance is particularly large because sector volume changes also contribute. The fit between the model and the peak daily counts in Fig. 8 is not as good as in the other two figures. This suggests that Equation (4), which relates altitude change fraction to conflict capacity via the effective vertical miss distance, does not capture the entire effect of the altitude change fraction. The availability of accurate altitude change information in the new SDAT data set revealed this problem for the first time. We are investigating the use of an additional recurring workload term to improve the altitude fit.

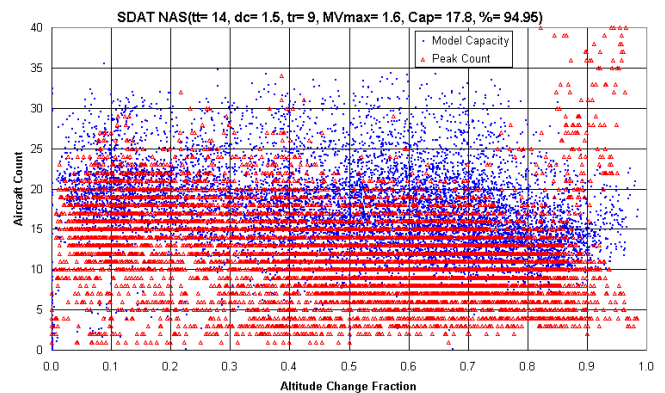


Figure 8.  $N_m$  and  $N_p$  versus versus altitude change fraction  $F_{ca}$ .

We have noted that Figs. 6, 7, and 8 all include outlier counts from TRACON sectors. We know that they are

TRACON sectors because the outliers cluster around sector volumes of 10,000 cubic nautical miles, transit times of 600 seconds, and altitude change fractions of 0.9. These are all attributes of terminal airspace.

### F. Regression Accuracy

Fig. 9 is the distribution of the difference between the rounded model capacity  $N_m$  and the peak count  $N_p$  for the current regression parameters. The mean is 5.6 aircraft, the variance is 39.4 aircraft, and there are 415 (4.8% of the total) instances of perfect matches ( $N_m = N_p$ ). As the fit quality improves, the mean and variance drop, and more perfect matches occur. The equivalent numbers for a good (transit service time  $\tau_r = 30$  s, 98.5 percentile) MAP model regression fit against the SDAT NAS data are significantly inferior: mean = 17, variance = 204, and perfect match count = 47.

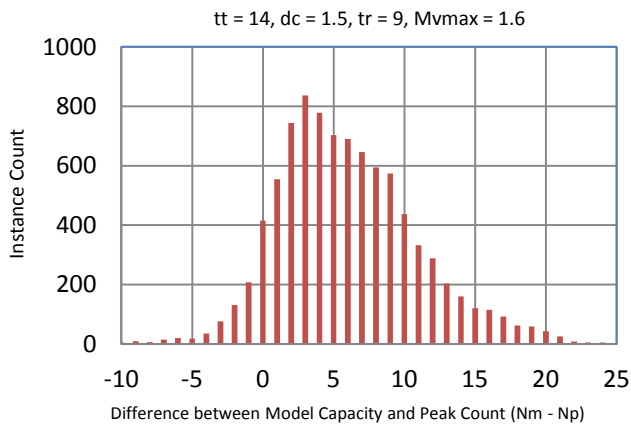


Figure 9. Distribution of difference between  $N_m$  and  $N_p$ .

The 2-D histogram of Fig. 10 provides another view of the distribution of NAS sectors relative to the capacity frontier. The figure shows the number of instances of each combination of observed peak count and capacity rounded to integer values.

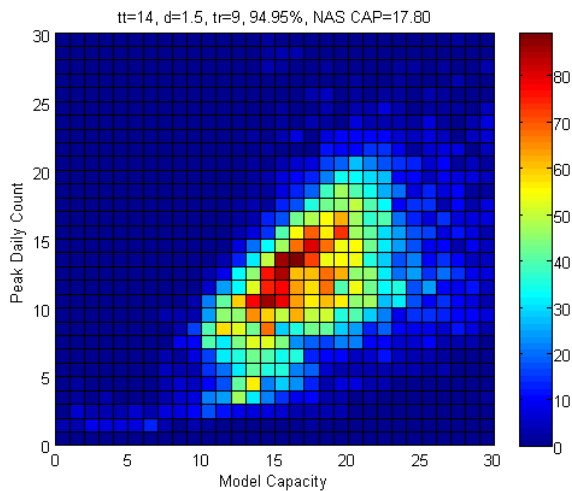


Figure 10. 2-D histogram of peak count and model capacity.

The 95-percentile fit is well aligned with the histogram axes, and the frontier is extended and linear with uniform

counts. It is consistent with Fig. 9, in that most peak counts fall between two and four aircraft below their corresponding model capacities. The bin with the highest count (102 instances) corresponds to a model capacity of 14 aircraft and a peak count of 10 aircraft.

We expect the addition of a new term relating recurring workload to altitude change fraction to result in a regression with improved accuracy and better overall agreement between the peak count frontiers and the data spreads of the model capacities and the peak daily counts.

### G. Parameter Ambiguity

Because the model has extra degrees of freedom, multiple parameter combinations exist that give nearly identical sector capacities. One can resolve ambiguity technically by quantizing the search parameters and by fitting the model to many sector count observations, which are naturally quantized to integer values. Given enough sector data, a quantized regression always returns a unique global peak.

However, ambiguities remain in the form of local peaks in the regression score. Local peaks produce nearly identical sector capacities, and thus do not reduce confidence in the model's capacity predictions. However, prominent local peaks can have distinctly different workload component ratios. If there were a reason to select a peak other than the global peak, it could alter predictions of the benefit of reducing a specific workload type.

The ambiguity between transit and conflict workload is illustrated in Fig. 11, which is a contour plot of the scores from an earlier regression. The maximum score occurred with a transit service time of  $\tau_r = 13$  seconds, a mean conflict separation loss of  $d_c = 1.6$  nautical miles, and a recurring service time of  $\tau_r = 9$  seconds. In the plot, the recurring service time is fixed at  $\tau_r = 9$  seconds, and the transit service time  $\tau_r$  and conflict separation loss  $d_c$  are integer independent variables.

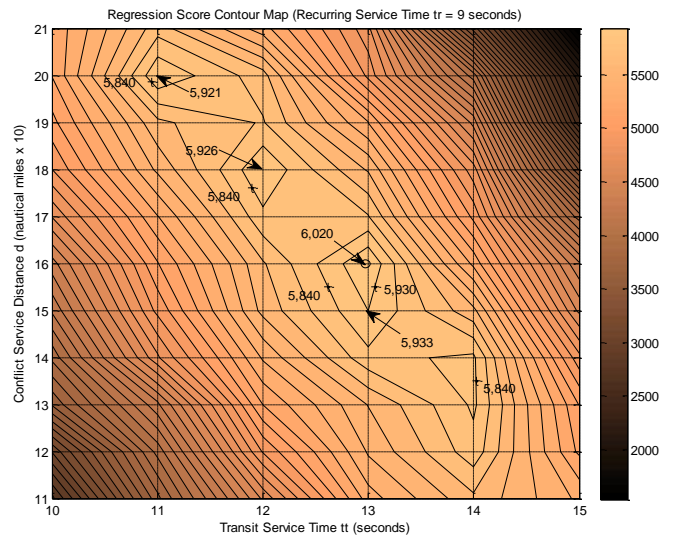


Figure 11. Contour plot of score with constant recurring service time.

Each grid intersection node in the plot represents a unique parameter set with a discrete integer regression score. The scores are interpolated to generate the contours. The interval between contours is a score difference of 90, and for clarity, we label only the two highest contours (5,840 and 5,930). The text arrows indicate the locations of the four highest scores.

The peak score (6,020) occurs at  $\tau_t = 13$  seconds and  $d = 1.6$  nautical miles and is indicated with a small circle. The second largest score (5,933) occurs at the node directly below the peak.

The ridge of peaks indicates a nearly linear inverse trade-off between transit service time and conflict service distance when recurring service time is held constant. Similar inverse trade-offs occur between other parameter pairs.

The local peaks in Fig. 11 all have scores and capacities that are close to those of the global peak. However, some of them represent significant changes in local parameter combinations and thus imply significantly different transit and conflict workload intensities.

We can compute the effect of hypothetical changes in workload parameters by averaging sector capacities and sector workload intensity components over all of the NAS sectors. Moving along the peak contour ridge from “northwest” ( $\tau_t = 11$ ,  $d = 2.0$ ) to “southeast” ( $\tau_t = 14$ ,  $d = 13$ ), the mean NAS capacity changes by only 2%, but the mean NAS conflict workload intensity drops by 34% and the mean NAS transit workload intensity increases by 24%. These changes in workload intensity reflect significant changes in the service time parameters.

Although this regression ambiguity reduces the confidence with which one can distinguish between workload types in a critical benefits analysis, there is usually no practical reason for choosing any of the local peaks over the global peak. The regression score provides a unique basis for choosing between the competing parameter sets. The fact that the second highest score is a single integer step away from the global peak (and also satisfies the 95-percentile goal) increases our confidence that the global peak provides a reasonably valid estimate for the NAS workload intensity components.

Nevertheless, the entire regression process is based on a cost function that employs arbitrary reward and penalty parameters. The regression cost function is “objective” only in the sense that it converges to a quantitative goal by returning a unique global peak score.

One can change that goal and its resulting solution set of model parameters in several ways. We routinely vary the award/penalty ratio to seek an arbitrary percentile objective. The solution changes when we regress against data sets based on different peak traffic observations. We find large differences in the solution sets when regressing against data derived from individual en route centers in the NAS [13].

The excess degrees of freedom in the model can be useful when extending, modifying, or improving it to handle new discoveries (such as the poor altitude change fraction fit) or new applications, such as hazardous weather. However, when used in benefits studies, it is important to remember that its

predictions reflect ambiguous conclusions that are based on subjective choices.

### III. EXTENSION TO HAZARDOUS WEATHER

This section reviews and illustrates the extension of the model to estimate operational reductions in sector capacity resulting from hazardous weather blockage. A weather avoidance field (WAF) [22] derived from gridded weather forecast data [23] is used to compute the fractional weather volume blockage in each sector. The blockage fraction is then used to estimate sector workload growth and the resulting reduction in sector capacity relative to its fair weather capacity.

#### A. Weather-Impacted Workload Growth

The weather-impacted sector capacity estimation is defined by the following equation:

$$G = G_b + (\tau_r + \tau_{wr}F_w)\frac{N}{P} + (\tau_t + \tau_{wt}F_w)\frac{N}{T} + \frac{BN(N+1)}{Q(1-F_w)}. \quad (10)$$

This equation adds new workload terms to the fair weather workload intensity equation. The additional recurring controller time consumed per aircraft rerouted around weather is  $\tau_{wr}$ ,  $F_w$  is the fraction of the sector volume blocked by convective weather, and  $\tau_{wt}$  is the additional coordination time needed per weather-impacted sector hand-off.

The term  $F_w$ , which is the fraction of sector airspace volume blocked by weather is computed by integrating the weather avoidance field over the sector volume. We postulate that the additional service times are proportional to  $F_w$  and  $N$ . Because  $\tau_{wr}$  and  $\tau_{wt}$  are both unknown, we deduce their values by fitting the model to the sector peak counts during weather events.

#### B. Computation of Weather Blockage Fraction

From en route WAF data and 3D sector coordinates we compute the fractional volume blockage  $v_m$  using horizontal slices of gridded WAF data specified at  $N_h$  altitudes. Currently  $N_h = 4$  and the altitudes are  $h_n = 27, 31, 35, \text{ and } 39$  kft.

We define the sector coordinates as a set of horizontal modules with constant horizontal shape over a given altitude span. We vertically integrate the weather blockage inside all modules using the WAF values given at the four altitudes.

The fractional sector volume blockage is given by

$$F_w = \frac{\sum_{m=1}^M v_m}{\sum_{m=1}^M V_m}, \quad (11)$$

where  $M$  is the number of sector modules, the numerator is the volume within the sector that is effectively blocked by weather, and the denominator is the total sector volume. Each module has a volume given by

$$V_m = A_m \Delta H_m, \quad (12)$$

where  $A_m$  is the horizontal module area and  $\Delta H_m$  is the module altitude thickness.

#### C. Mean Fair Weather Transit Time

There are several alternative approaches to estimating mean fair weather sector transit time.

Because sector definitions as well as wind and flow patterns change dynamically, the most accurate approach is to predict mean transit time from filed flight plans and current airspace definitions. Historical averages or periodically updated sample measurements can be used when accuracy is less critical.

For simple alerting applications in which sector airspace definitions are a significant determinant of transit time, one can relate transit time to the sector size (given as its linear horizontal dimension). The relationship is

$$T_0 = C_T \sqrt{A_e}, \quad (13)$$

where  $A_e$  is the effective horizontal area of the sector and  $C_T$  is a constant determined by regression to mean fair-weather transit times for many sectors during peak daily traffic periods.

#### D. Weather-Impacted Transit Time

The forecast of  $T$  starts with an estimate of the fair-weather mean sector transit time,  $T_0$ , as noted above.

When the weather blockage  $F_w$  increases,  $T$  tends to decrease below  $T_0$  as weather forces flights to exit the sector.

In the limit, when the sector is completely blocked,  $T$  falls to zero. We have determined the following empirical relationship between  $T$  and  $T_0$ ,

$$T = (1 - \beta F_w)(1 - F_w^\gamma) T_0, \quad (14)$$

where currently  $\beta = 0.32$  and  $\gamma = 8$ .

#### E. Weather Model Regression

We regressed the model individually to determine unknown values of the additional service times  $\tau_{wr}$  and  $\tau_{wt}$  by fitting the model to the sector peak counts during weather events. We examined events in which hazardous weather developed in sectors that were operating at or near capacity.

Fig. 12 shows the results of a regression for  $\tau_{wr}$  and  $\tau_{wt}$  based on observed traffic collected over 28 days, from eight en route centers. We found the heaviest and most frequent impacts in ZOB and ZDC, yet the majority of weather coverage resulted in less than 50% weather blockage.

The vertical axis in the figure is  $\tau_w$  (defined as  $\tau_{wt} + \tau_{wr}$ ) and the horizontal axis is the percentage of  $\tau_w$  that is  $\tau_{wr}$ . The white "x" indicates the peak and shows that the additional coordination service time of  $\tau_{wt} = 60(0.2) = 12$  seconds and the additional recurring service time of  $\tau_{wr} = 60(0.8) = 45$  seconds yield the best regression results.

The weather model results are summarized in Fig. 13, which plots normalized sector capacity, that is, weather-impacted capacity divided by the constant fair-weather capacity, as a function of the weather blockage fraction.

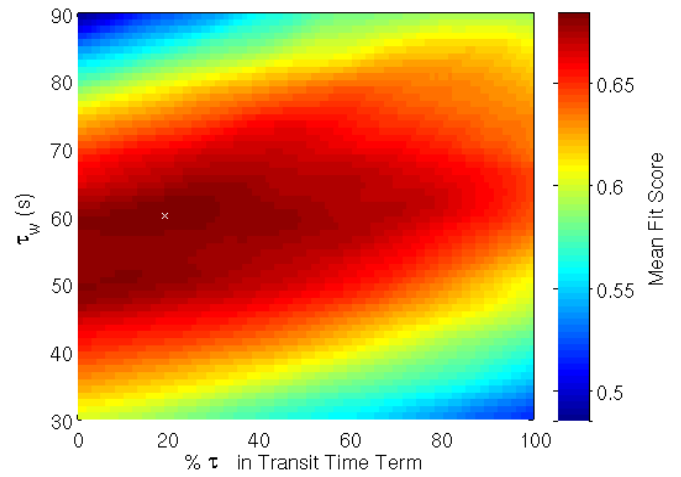


Figure 12. Weather model regression results.

Fig. 13 illustrates the normalized relationship for three different sector sizes. Here we assume that the sectors are of fixed height so that their mean transit times vary as the square root of the sector volume. This figure accounts for the growth in recurring service time, the linear decrease in mean transit time, and the reduction in usable sector volume with increasing weather blockage.

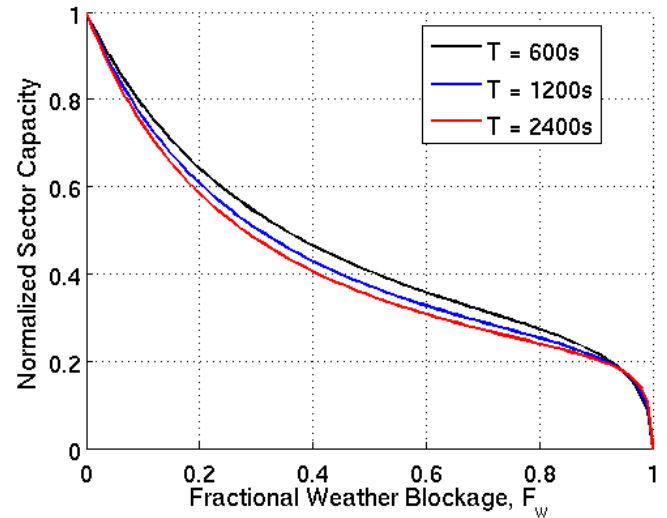


Figure 13. Normalized capacity model results.

Sector capacity declines in a roughly exponential manner until the blockage exceeds 0.8 and the resulting growth in traffic density causes conflict workload to dominate. The capacity then drops sharply to zero when the sector is totally blocked.

These normalized curves are relatively insensitive to transit time because transit time variations have roughly the same effect on fair-weather capacity as weather-impacted capacity. This is a significant result because it indicates that accurate knowledge of transit time is unnecessary for applications based on normalized capacity.

### F. Application of the Weather Blockage Model

We conclude with an illustration using archived traffic and weather data to simulate a procedure to add weather alerts to existing alerts based on en route sector demand. The procedure adds two sector hazardous weather alert flags to an existing alerting display. These flags would forecast hazardous weather capacity reduction with a 2-hour horizon.

In order to minimize distracting display fluctuations as forecast instability increases with look-ahead time, a smoothing algorithm is implemented. As the look-ahead time for forecasts increases, the required forecast persistence is also increased. Forecast persistence is the number of consecutive forecast weather blockage updates required *below* a weather alert threshold before dropping the forecast weather alert flag associated with that threshold. Currently, the persistence values are set to 1 (< 60 min look-ahead), 2 (60-90 minute look-ahead), and 3 (> 90 minute look-ahead).

Fig. 14 illustrates the performance of the procedure. The top panel shows the weather blockage fractions for the observed (black), 1-hr forecast (blue), and 2-hr forecast (red) vs. time. In the next three panels, the actual peak sector aircraft count (per 15-minute bin) is plotted in blue. The red curves are the model-generated normalized sector capacity estimates. The bottom plot shows the progression of the alerts in 15-minute intervals as a function of forecast time, where blue dots indicate a normalized capacity estimate of 50-75%, and red indicates a normalized capacity estimate of 0-50%. The estimates are reasonably timely, accurate, and stable.

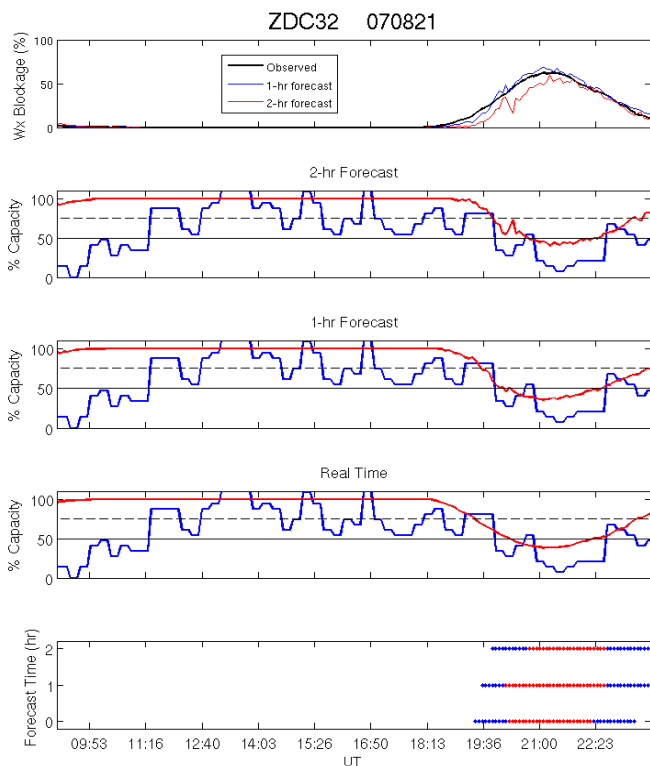


Figure 14. Simulation of sector hazardous alert concept.

### IV. CONCLUSIONS

The FAA's current operational en route capacity model is based on workload, bases its sole empirical parameter on peak traffic counts, and provides accurate capacity estimates for many en route sectors in fair weather.

It has served as the basis for a new expanded model, which aggregates workload into four basic types and obtains parameters by fitting to traffic counts, but which predicts capacity more accurately for all sectors, in all weather, and with enough workload specificity for quantitative benefits analyses.

We plan to further refine the model with a term relating recurring workload to altitude change fraction. We expect this to result in a regression with improved accuracy and better overall agreement between model capacities and peak daily counts.

### ACKNOWLEDGMENT

We would like to thank Joseph Post and Omar Baradi of the FAA for supporting this work.

### REFERENCES

- [1] J. Welch, J. Andrews, B. Martin, and B. Sridhar, "Workload model for estimating en route sector capacity," 7th USA/Europe ATM R&D Seminar, Barcelona, Spain, 2007.
- [2] J. Y. N. Cho, J. D. Welch, and N. K. Underhill, "Analytical workload model for estimating en route sector capacity in convective weather," 9th USA/Europe ATM R&D Seminar, Berlin, Germany, 2011.
- [3] J. Post, M. Wells, J. Bonn, and P. Ramsey, "Financial Incentives for NextGen Avionics, ADS-B Case Study," 9th USA/Europe ATM R&D Seminar, Berlin, Germany, 2011.
- [4] M. Bennett, D. Knorr, and J. Rakas, "Economic benefits of an increase in en route sector capacity from controller-pilot data link communications," *Transportation Research Record*, vol. 1888, 2004.
- [5] L. Song, D. Greenbaum, and C. Wanke, "The impact of severe weather on sector capacity," 8th USA/Europe Air Traffic Management R&D Seminar, Napa, CA, 2009.
- [6] J. Krozal, J. S. B. Mitchell, V. Polishchuk, and J. Prete, "Capacity estimation for airspace with convective weather constraints," 9th AIAA Aviation, Technology, Integration, and Operations Conf., Hilton Head, SC, September 2009.
- [7] Federal Aviation Administration, "Monitor alert parameter," Air Traffic Organization Policy Order JO 7210.3W, U.S.DOT, Washington, DC, 2010, [http://www.faa.gov/air\\_traffic/publications/atpubs/fac/1708.html](http://www.faa.gov/air_traffic/publications/atpubs/fac/1708.html).
- [8] J. D. Welch, J. W. Andrews, B. D. Martin, and E. M. Shank, "Applications of a macroscopic model for en route sector capacity," AIAA Guidance, Navigation, and Control Conf., Honolulu, HI, August 2008.
- [9] M. Robinson, R. A. DeLaura, B. D. Martin, J. E. Evans, and M. E. Weber, "Initial studies of an objective model to forecast achievable Airspace Flow Program throughput from current and forecast weather information," Project Rep. ATC-343, MIT Lincoln Laboratory, Lexington, MA, 52 pp., 2008.
- [10] A. Klein and L. Cook, "Three models for weather impacted airspace capacity estimation and forecast", 9th USA/Europe ATM R&D Seminar, Berlin, Germany, 2011.
- [11] B. Martin, "Model estimates of traffic reduction in storm impacted en route airspace," 7th AIAA Aviation, Technology, Integration, and Operations Conf., Belfast, Ireland, 2007.
- [12] D. K. Schmidt, "A queuing analysis of the air traffic controller's work load," *IEEE Trans. Systems, Man, Cybernetics*, vol. SMC-8, pp. 492-498, June 1978.

- [13] J. D. Welch and J. W. Andrews, "Macroscopic capacity model with individual sector closing speed estimates," 9<sup>th</sup> AIAA Aviation, Technology, Integration, and Operations Conf., Hilton Head, SC, September 2009.
- [14] J. Welch, J. Andrews, and J. Post, "Validation of en route capacity model with peak counts from the US National Airspace System," EN-012, 2<sup>nd</sup> ENRI International Workshop on ATM/CNS, Tokyo, Japan, 2010.
- [15] K. Geisinger and B. MacLennan, "Sector Design Analysis Tool (SDAT) workload model design document," Operations Research Service, AOR-200, Federal Aviation Administration, 1994.
- [16] B. Sridhar, K. S. Seth, and S. Grabbe, "Airspace complexity and its application in air traffic management", 2nd USA/Europe ATM R&D Seminar, Orlando, December 1998.
- [17] G. Donahue, "A Simplified Air Transportation System Capacity Model", Journal of ATC, April-June 1999.
- [18] D. Delahaye and S. Puechmorel, "Air traffic complexity: towards intrinsic metrics," 3rd USA/Europe ATM R&D Seminar, Napoli, Italy, June 2000.
- [19] G. B. Chatterji and B. Sridhar, "Measures for air traffic controller workload prediction, "1st AIAA Aircraft Technology Integration and Operations Forum, Los Angeles, CA, 2001.
- [20] A. Majumdar, W. Ochieng, and J. Polak, "Estimation of European airspace capacity from a model of controller workload," J. Navigation, vol. 55, pp. 381-403, 2002.
- [21] P. Kopardekar, A. Schwartz, S. Magyarits, and J. Rhodes, "Airspace complexity measurement: An air traffic control simulation analysis," 7th USA/Europe Air Traffic Management R&D Seminar, Barcelona, Spain, July 2007.
- [22] R. A. DeLaura, M. Robinson, M. L. Pawlak, and J. E. Evans, "Modeling convective weather avoidance in enroute airspace," 13<sup>th</sup> AMS Conf. on Aviation, Range, and Aerospace Meteorology, New Orleans, LA, 2008.
- [23] J. E. Evans and E. R. Ducot, "Corridor Integrated Weather System," Linc. Lab. J., vol. 16, pp. 59-80, 2006.

#### AUTHOR BIOGRAPHY

**Jerry D. Welch** holds a B.S. and M.S. (1960) from MIT and a Ph.D. (1973) from Northeastern University in electrical engineering.

He is a Senior Staff member in the Surveillance Systems Group at MIT Lincoln Laboratory in Lexington, Massachusetts (1962-present). He

helped establish the team that developed the Mode S beacon system for the FAA. He initiated the Traffic Alert and Collision Avoidance System surveillance program. He organized an Air Traffic Automation Group that helped establish programs in Terminal ATC Automation and Runway Status Lights.

Dr. Welch is a member of the American Institute of Aeronautics and Astronautics.

**John Y. N. Cho** holds a B.S. (1985) and M.S. (1986) from Stanford University and a Ph.D. (1993) from Cornell University in electrical engineering.

He is a Senior Staff member in the Weather Sensing Group at MIT Lincoln Laboratory (2002-present). He was a Research Scientist in the Earth, Atmospheric, and Planetary Sciences Department at MIT (1997-2002), a Research Associate at the Arecibo Observatory (1993-1997), and a Visiting Scientist at the Leibniz Institute for Atmospheric Physics (summer 1996). He has 46 refereed publications.

Dr. Cho is a member of the American Meteorological Society and the American Geophysical Union.

**Ngairé K. Underhill** holds a B.S. (2008) from Smith College in computer science and economics, and a M.P.S. (2011) in information science from Pennsylvania State University.

She is an Associate Staff member in the Weather Sensing Group at MIT Lincoln Laboratory (2008-present). Her other work includes analyses on weather conditions for departure routes for aircraft particularly involving the Route Availability Planning Tool, air traffic flow patterns, and aircraft rerouting optimization, and terminal operations.

Ms. Underhill is a member of the American Meteorological Society.

**Richard A. DeLaura** holds an A.B. (1977) in chemistry and physics from Harvard University.

He is a Staff Scientist in the Weather Sensing Group at MIT Lincoln Laboratory (2000-present). He has authored or co-authored several conference proceedings and FAA research reports, and is currently responsible for several research efforts investigating the impacts of adverse weather on air traffic operations. Prior to his current work at Lincoln Laboratory, he was a Research Scientist at University of Massachusetts, Dartmouth, developing software and curriculum to introduce advanced mathematical concepts to middle and high school students.